

Initiation and evolution of pancake ice in a wave field

GREGORY H. LEONARD *and* HAYLEY H. SHEN, *Department of Civil and Environmental Engineering, Clarkson University, Potsdam, New York 13699*

STEVEN F. ACKLEY, *Snow and Ice Division, U.S. Army Cold Regions Research and Engineering Laboratory, Hanover, New Hampshire 03755*

Waves are ubiquitous in the southern oceans. Their presence has been linked to the predominant pancake-ice formation in the antarctic marginal ice zone. The morphology of an ice cover formed from a pancake ice field is determined by the initial pancake floe's size and thickness. The incorporation of any biological material into an ice cover also begins with this initial formation. No systematic field observations have been made of this formation process. This article describes a laboratory study in which various wave fields, with or without wind and current, were created in a refrigerated recirculating flume. The evolution of the resulting ice covers clearly depends on these hydrodynamic conditions.

Six ice-growth tests were conducted in the Hamburg Ship Model Basin in Hamburg, Germany. The parameters are shown in the table. The instruments used for these tests included a pressure transducer, an infrared videocamera, and a regular videocamera. The pressure transducer was placed in the middle section of the tank. This pressure transducer traversed a length of the tank along at least 10 locations, and the separation between locations was 15 centimeters. Time series were taken at these locations, from the paddle side down, one at a time. Each time series consists of 1,024 readings at 50-hertz data rate. A 30-second infrared video image and regular video image were recorded after each session of pressure-data

acquisition. All three recordings were done at roughly a 30-minute interval.

In these tests, test B had very high wave amplitude in which ice crystals were swept down from the paddle to the extent that most of the test section was open water throughout the test duration. The remaining tests are separated into two: C, D, and E were under wave-only conditions and A and F had wind (with or without current) in addition. The presence of wind greatly changes the morphology of the ice cover as will be discussed below.

The results are summarized in terms of time evolution of wave amplitude under the ice cover and the observation of the ice-cover evolution. An example of these results is given in the figure. The wave energy is attenuated by the ice cover as it grows, but the amount of attenuation depends on the type of the ice cover, which changes with time.

Although the number of tests conducted is low compared with the number of variables observed, some general trends can be observed in these three tests.

- The diameters of the pancakes are on the order of 1/100 of the dominant wavelength.
- The evolution of a pancake ice cover from grease ice is dependent on the wave condition. Gentle waves produce pancakes that will evolve into composites. Energetic waves

Parameters of six ice-growth tests

	A	B	C	D	E	F
Air temperature ^a	-11 to about -12.5	-11 to about -15.5	-10 to about -16	-13.5 to about -15.5	-11 to about -13.5	-6 to about -11
Wave frequency	.48/.96	.73	.71	.53/1.07	.7	.7
Wave amplitude	Low	High	Medium	Medium	Medium	High
Wind ^b	6 to more than 4.5	None	None	None	None	6 to more than 4.5
Current ^c	None	None	None	None	None	10

^aIn °C.
^bIn meters per second.
^cIn centimeters per second.

produce more irregular, and thicker, pancakes that remain dispersed.

- Wave attenuation by an ice cover depends on the type of ice cover. The attenuation efficiency of grease ice increases with ice thickness. The onset of pancakes lessens the attenuation and the onset of composite pancakes increases the attenuation.

Wind has a definitive effect on the formation of ice cover because it creates frazil at a much higher rate so that grease-ice production is prolonged and pancake-ice formation is hindered. In tests A and E, the ice cover remained slushy. Only toward the end of the tests were some sparsely distributed pancakes able to form above a very thick layer of frazil.

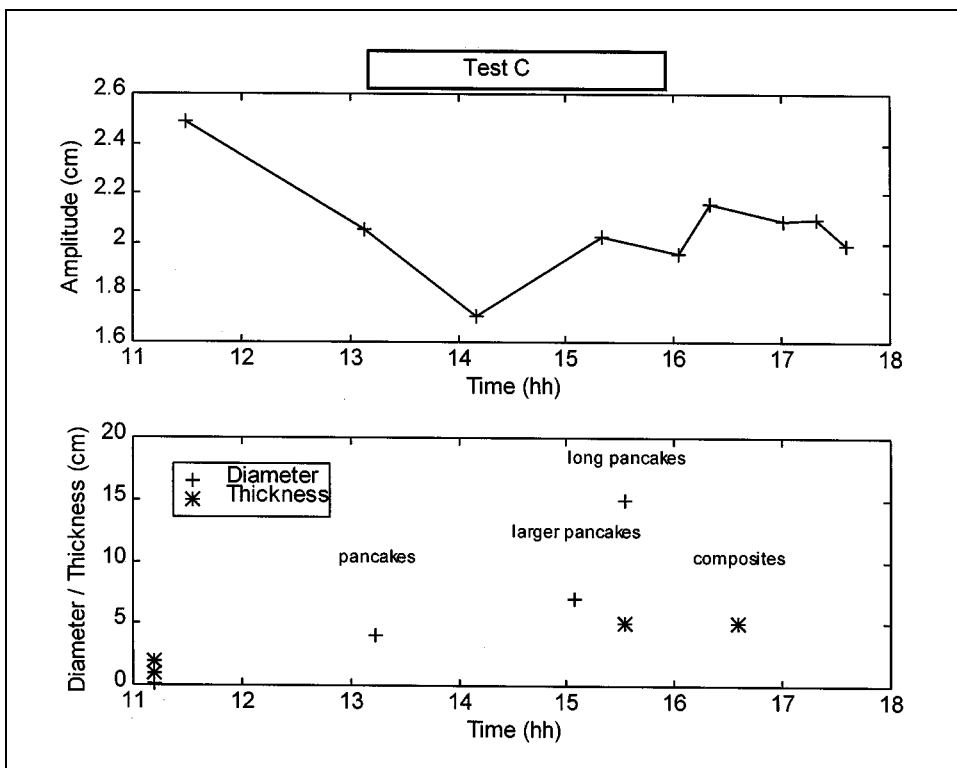
The microstructure of the ice cover was also observed. The initial crystals before a well-defined grease-ice layer formed were flakelike. Their size was about 1 centimeter in diameter in all these tests. Such crystals went through a rapid kinetic growth under super-cooled conditions. Well-defined pancakes consist of a frozen top and a slushy bottom. The slush is an agglomerate of platelets of several millimeters in diameter stacked up horizontally. These platelets are formed from the initial frazils rubbing against and freezing onto each other due to the oscillatory motion in the wave field. The rubbing causes the initial crystals to lose their dendritic offshoots and to reduce their sizes. The horizontal orientation indicates the possibility of highly anisotropic permeability in the ice cover that is subsequently formed by these pancakes.

From these tests, it is suggested that the dynamic formation of an ice cover in a wave field may be described by four stages.

- *Grease-ice stage.* Frazil disks having dendritic offshoots form in super-cooled water. As their number increases and as they float and accumulate on the water surface, they form a thicker and thicker layer. In this layer, crystals erode away their edges and freeze together to form round platelets.
- *Primary pancake stage.* As the platelets form, the accumulation of the total ice forces the top part of the grease ice to be exposed to cold air. Instantaneous fusion between neighboring platelets takes place over the whole ice-cover surface. Concomitantly, bending from the waves cracks the ice sheet into primary pancakes. The size of these primary pancakes depends on the high-frequency part of the wave spectrum.
- *Maturing pancake stage.* The accumulation of ice on the water surface damps away the high-frequency part of the wave. The remaining longer waves now work on the lateral fusion of primary pancakes to form mature pancakes. This maturing process is a competition between the vertical growth of existing pancakes due to wave compaction and rafting and the lateral growth of pancakes by accumulating more frazil. If the vertical growth is more rapid, only slushy ice cover will persist. If the lateral growth is more rapid, well-defined pancakes will form.

- *Composite-pancake stage.* If the lateral growth overrules, a field of well-defined pancake ice floes will form throughout the surface. The differential motion of neighboring pancakes in a wave field has a chance to bring floes together. Under cold air, the exposed part of floes will freeze to form composites. The extent of floe composition is limited by the wavelength.

Provided that the above scenario is correct, it is clear that the morphology of an ice cover is a product of the thermodynamic and hydrodynamic conditions prescribed by air temperature and by the wind, wave, and current conditions. Of the latter three, wind produces waves, especially the high-frequency spectrum part. Wind also promotes heat loss and frazil production rate. Waves shape the platelets formed from the initial crys-



A sample test result

tals, promote vertical growth of these platelets by rafting and compaction, and create lateral growth of mature pancakes by fusion through differential motion of pancakes. On top of these, air temperature is a key factor that highly influences the initial frazil production and the late fusion rate. Finally, current may determine the frazil distribution in the water through the

induced turbulence and, thus, the surface accumulation efficiency.

This research was supported by National Science Foundation grants OPP 93-15934 and OPP 92-19165 as well as by the National Science Foundation's International Program. Technical support from the Hamburg Ship Model Basin, Hamburg, Germany, is deeply appreciated.

Describing the composition of sea-ice cores and the development of the antarctic sea-ice cover

MARTIN O. JEFFRIES, *Geophysical Institute, University of Alaska–Fairbanks, Fairbanks, Alaska 99775–7320*

Sea-ice thickness plays a key role in ocean-atmosphere interactions (exchanges of heat, mass, and momentum) and thus regional and global climate variability. The thickness of the sea-ice cover is determined by thermodynamic (freezing, melting) and dynamic (deformation) processes. Information on some of these processes can be obtained from the analysis of the ice-crystal texture and the stable isotopic composition of ice cores.

The ice-crystal texture and stable isotope composition of sea ice depend on the growth mechanism and the conditions under which it occurs. In calm conditions, congelation ice, which grows at the base of an ice floe as heat is conducted upward to the surface, develops a columnar texture of elongated crystals. In turbulent conditions, such as at the surface of a wind- and wave-roughened sea, rapid freezing creates frazil ice crystals that have a granular texture. Snow ice, which forms after seawater has flooded the ice/snow interface, also has a granular texture. Because of their similar textures, frazil ice and snow ice are identified on the basis of differences in stable isotopic composition (Lange et al. 1990).

Congelation ice, frazil ice, and snow ice are the most common types observed in antarctic sea-ice floes. The figure illustrates the amounts in which they occurred in four ice cores obtained from the same first-year ice floe (number 247–95). The amount of each ice type differs in each core, and the cores have different lengths. This variability is a common characteristic of antarctic sea ice and reflects the complex history of the floe, which had thickened by different combinations of thermodynamic and dynamic processes as a number of smaller floes agglomerated over time and under changing conditions.

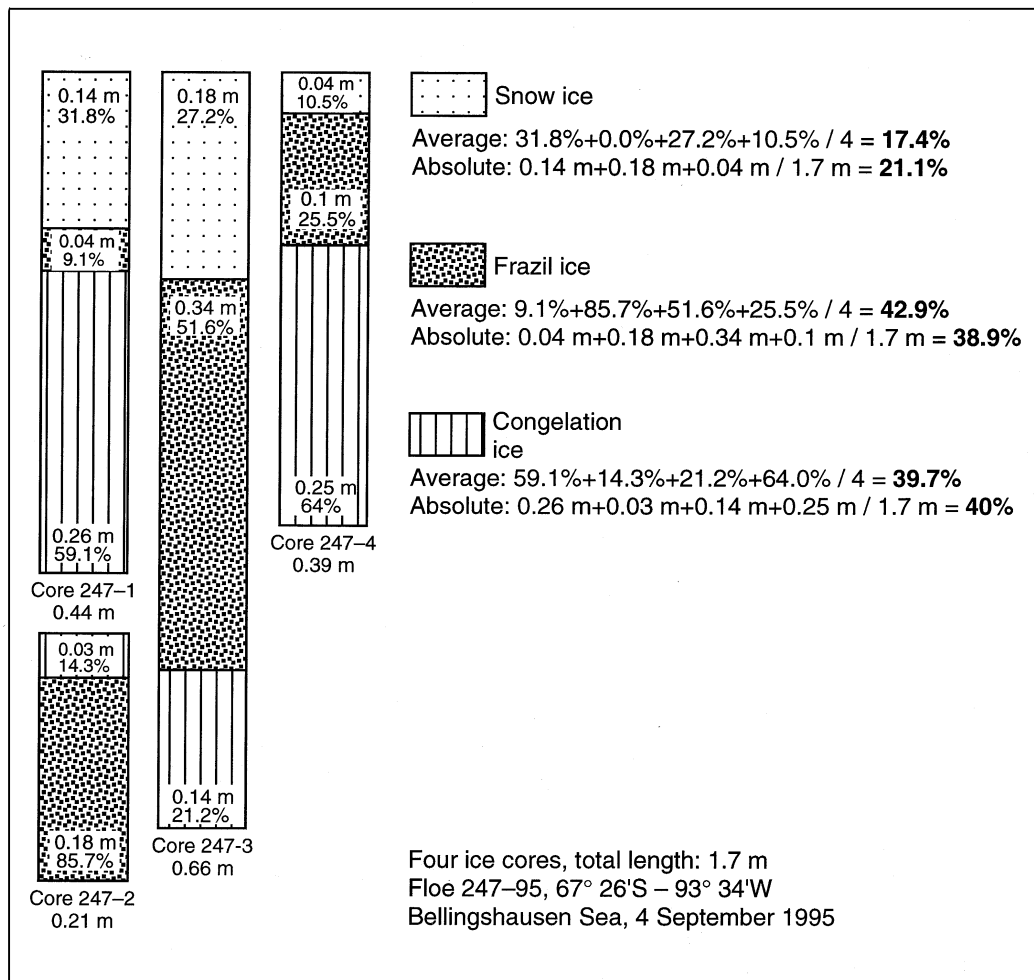
Based on measurements made at 151 drill holes, floe 247–95 had a mean thickness of 0.43 meters (m) and range of 0.2–0.75 m. The four ice cores had a mean length of 0.425 m and range of 0.21–0.66 m. The cores, then, are reasonably repre-

sentative of the thickness variability of the floe. Assuming that the ice types observed in the cores are also representative of the entire floe, the contribution of each ice type to the development of the floe is determined from the combined composition of the four cores.

There are two different methods for obtaining a measure of the contribution of ice types to the development of the ice cover: the *average* method and the *absolute* method, as illustrated in the figure. The *average* method adds the percentage amount of a particular ice type in each core and then divides that total by the number of cores to give an average percentage for that ice type. The *absolute* method adds the total amount (in meters) of a particular ice type measured in each core and then divides that total by the total length of the cores (in meters) to give an absolute percentage for that ice type.

While working aboard the R/V *Nathaniel B. Palmer* during four cruises in the Ross, Amundsen, and Bellingshausen Seas in May, June, August, September, and October 1993–1995, the composition of a total of 338 first-year ice cores with a total length of 253.71 m has been analyzed. Here, only the 282 cores (total length 219.09 m) obtained from the outer pack ice on the deep ocean north of the continental shelf are considered. The cores from the inner pack ice on the continental shelf are excluded because they contained an anomalously large quantity of congelation ice (approximately 65 percent; Jeffries and Adolphs 1997).

Whether one looks at a single floe (figure) or the entire winter pack-ice cover, the method of calculating the ice-core composition does not make a significant difference to the results, in this particular instance; the absolute and average amounts of each ice type are almost the same. For the set of 282 ice cores, the absolute amounts of snow ice, frazil ice, and congelation ice are 29, 37, and 31 percent, respectively. The average amounts of each ice type are 30, 34, and 35 percent,



Proportional representation of the amounts of snow ice, frazil ice, and congelation ice observed in four cores obtained from the same ice floe. Each column represents the total length of ice core examined normalized to 1 or 100 percent. The total amount of each ice type observed in each core is represented by the length of the space it occupies within the column. For example, a total of 0.18 m of snow ice was observed in core 247-3, representing 27.2 percent of the total core length of 0.66 m. The contribution of a particular ice type to the development of the floe is calculated by the *average* or *absolute* method, as illustrated to the right of the core diagrams.

respectively. Minor ice types that are of no consequence to this analysis make up the remaining 1-3 percent.

Whether one considers the absolute or the average amount of ice, the preponderance of frazil ice is consistent with observations in the Weddell Sea and the east antarctic pack ice (Lange and Eicken 1991; Worby et al. in press). The amount of frazil ice is smaller than elsewhere, however, because snow ice makes a greater contribution to pack-ice development than has been reported in the other antarctic pack-ice zones. The significant difference in congelation ice amounts on the deep ocean and the continental shelf suggests that these zones may have very different pack-ice regimes, as determined by atmospheric and oceanographic forces (Jeffries and Adolphs 1997).

The method that is chosen to calculate the contribution of each ice type may depend on the purpose of the study and the preference of the investigator, but I recommend that the *absolute* method be adopted as the standard, because it provides a better measure of the contribution of a particular ice type to the total volume or mass of the ice cover. Adoption of a standard would also make it easier to compare observations made by different investigators in different sea-ice zones. Failing this, I recommend that all authors at least clearly identify the method that they have used to describe the composition of their cores.

This work was made possible by National Science Foundation grants OPP 91-17721 and OPP 93-16767. I thank the many people who worked long hours with me on ice floes and in the science freezer aboard the ship. Captain Joe Borkowski, the mates, and crew of the R/V *Nathaniel B. Palmer* contributed to the success and enjoyment of the cruises.

References

- Jeffries, M.O., and U. Adolphs. 1997. Early winter snow and ice thickness distribution, ice structure and development of the western Ross Sea pack ice between the ice edge and the Ross Ice Shelf. *Antarctic Science*, 9(2), 188-200.
- Lange, M.A., and H. Eicken. 1991. Textural characteristics of sea ice and the major mechanisms of ice growth in the Weddell Sea. *Annals of Glaciology*, 15, 210-215.
- Lange, M.A., P. Schlosser, S.F. Ackley, P. Wadhams, and G.S. Dieckmann. 1990. ^{18}O concentrations in sea ice of the Weddell Sea, Antarctica. *Journal of Glaciology*, 36(124), 315-323.
- Worby, A.P., R.A. Massom, I. Allison, V.I. Lytle, and P. Heil. In press. East antarctic sea ice: A review of its structure, properties and drift. In M.O. Jeffries (Ed.), *Antarctic sea ice physical processes, interactions and variability* (Antarctic Research Series, Vol. 74). Washington, D.C.: American Geophysical Union.

Deep coastal oceanography from McMurdo Sound to Marguerite Bay

STANLEY S. JACOBS, *Lamont-Doherty Earth Observatory of Columbia University, Palisades, New York 10964*

Thirty years ago Lamont investigators made the first continuous vertical “STD” (salinity-temperature-depth) profiles in the Ross Sea, casting from the *Eltanin* with an early model of the now widely used “CTD.” The original acronym has long since been abandoned to the public health sector, and the “C” now stands for seawater conductivity, from which salinity is calculated (as is “D” from pressure). From the many “bottle” and CTD casts made in the Ross Sea before and since that time, a rough time series of summer temperature and salinity measurements can be compiled (Jacobs and Giulivi in press-a). Unlike local meteorological observations and satellite-derived information on sea-ice extent, the oceanographic data are highly discontinuous in space and time. In spite of geographical biases (e.g., Giulivi and Jacobs 1997a) and a curious year-round salinity record (from McMurdo Sound), it is apparent that interannual salinity variability is substantial on the Ross Sea continental shelf. The salinity changes are correlated with sea-ice range (figure 1), which has a periodicity of several years. Superimposed on the large short-term variability is a slight decline in shelf water salinity over the past four decades in the southwest Ross Sea (Jacobs and Giulivi in press-b).

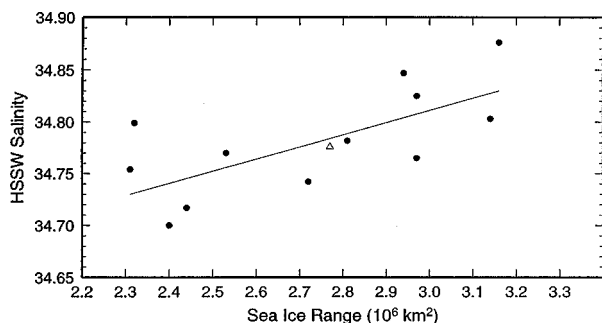


Figure 1. Average salinity at 450–550-meter depths in the High Salinity Shelf Water (HSSW) on the continental shelf in the western Ross Sea (160°E–180°E) versus sea-ice range the previous year. Each point represents salinity data for one summer, usually December through February, with sea-ice range calculated from the Ross sector preceding winter maximum minus the prior summer minimum. (km² denotes square kilometers.)

Over the past 150 years, even the area of the open Ross Sea continental shelf has changed. Continued monitoring of the position of the Ross Ice Shelf front (Keys, Jacobs, and Brigham in press) reveals that the western portion of the ice front is now more than 75 kilometers (km) north of its location in 1911, around the time that Amundsen and Scott trekked to the South Pole. The “B-9” iceberg released by the eastern ice front

in 1987 removed an area larger than the island between Manhattan and Montauk, but steady advance along the entire ice front since then has more than regained the ice shelf real estate lost in that calving event. The growth of the Ross and other ice shelves stands in contrast to well-publicized retreats along the Antarctic Peninsula and suggests that the circumpolar inventory of the shelf ice may be little changed in recent times.

Three years ago, on cruise 9402 of the *Nathaniel B. Palmer*, we made the first oceanographic measurements in some antarctic coastal regions between the eastern Ross Sea and Marguerite Bay (Giulivi and Jacobs 1997b). Using new Amundsen Sea data for validation, Hellmer, Jacobs, and Jenkins (in press) modeled the flow of circumpolar deep water beneath Pine Island Glacier, where the basal melt rate appears to exceed 10 meters per year (Jacobs, Hellmer, and Jenkins 1996). In combination with a calving rate obtained from radar satellite observations, that melting roughly balances the estimated flow of ice across the deep grounding line (Jacobs, Jenkins, and Hellmer 1996). Meltwater increases the dissolved oxygen content of the deep water that upwells beneath the glacier but lowers its oxygen isotope ($\delta^{18}\text{O}$) content, from which the $\delta^{18}\text{O}$ of precipitation on the glacier catchment basin can be inferred (figure 2). Relatively shallow and warmer than

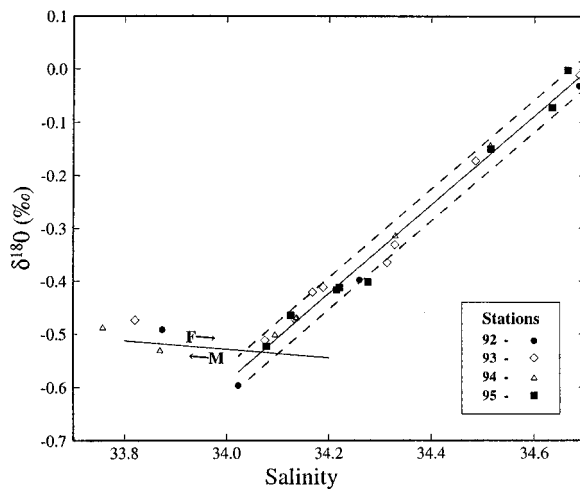


Figure 2. Oxygen isotope/salinity diagram for stations in Pine Island Bay (74°50'S 102°40'W) in the southeast Amundsen Sea. The solid line fit to the deeper samples extrapolates to a zero-salinity $\delta^{18}\text{O}$ content near -29‰ , the probable mean value for precipitation on the Pine Island Glacier (75°10'S 100°00'W) catchment basin. Dashed lines indicate the precision of $\delta^{18}\text{O}$ measurements by S. Khatiwala at Lamont-Doherty.

the ambient environment, outflows from beneath the glacier are likely to influence local sea-ice formation.

Following up on an earlier finding of higher seabird populations near the Antarctic Slope Front, Ainley et al. (in preparation) evaluated bird distributions observed during *Palmer* cruise 9402, late enough in the season that summer colonies had been abandoned. They found that ocean thermohaline fronts in the Amundsen and Bellingshausen regions are more diffuse and less related to the continental shelf break than in the Ross Sea. Interpretations were complicated by overly wide ocean station spacing, by the lack of prey data and unavoidable time gaps in the observations, and by large flocks of birds roosting by day and feeding at night. It remains to be determined how deep subsurface features compete with or enhance the ice-edge environment as a magnet for top-gun predators.

From the limited historical ocean data available, it is difficult to determine whether significant temporal changes have occurred in waters on the Southeast Pacific antarctic continental shelf. Nearly 100 years ago, oceanographic measurements were made from the *Belgica*, beset for more than a year in the close pack of the southern Bellingshausen Sea. Their southernmost temperatures are substantially colder than the *Palmer* CTD profile at the same location (figure 3): a deep temperature maximum in March approximately 0.3°C below that of our March 1994 data. Ongoing analyses of such compar-

isons may allow any long-term temperature trend to be separated from the short-term variability.

C. Giulivi and H. Hellmer assisted with data reduction and figures. This research was supported by National Science Foundation (OPP 94-18151), with assistance from the National Aeronautics and Space Administration (NAGW-1344), the Department of Energy (DE-FG02-93ER61716), and Lamont-Doherty Earth Observatory.

References

- Ainley, D.G., S.S. Jacobs, C.A. Ribic, and I. Gaffney. In preparation. Seabirds and oceanic features of the Amundsen and southern Bellingshausen Seas, late summer-early autumn 1994. *Antarctic Science*.
- Giulivi, C.F., and S.S. Jacobs. 1997a. *A zonal oceanographic section in the southern Ross Sea: Oceanographic data taken from the USCGC Polar Sea, February 1994* (Technical Report 97-2). Palisades, New York: Lamont-Doherty Earth Observatory.
- Giulivi, C.F., and S.S. Jacobs. 1997b. *Oceanographic data in the Amundsen and Bellingshausen Seas: N.B. Palmer cruise 9402, February-March 1994* (Technical Report 97-3). Palisades, New York: Lamont-Doherty Earth Observatory.
- Hellmer, H.H., S.S. Jacobs, and A. Jenkins. In press. Oceanic erosion of a floating antarctic glacier in the Amundsen Sea. In S. Jacobs and R. Weiss (Eds.), *Ocean, ice, and atmosphere: Interactions at the antarctic continental margin* (Antarctic Research Series, Vol. 75). Washington, D.C.: American Geophysical Union.
- Jacobs, S.S., and C.F. Giulivi. In press-a. Thermohaline data and ocean circulation on the Ross Sea continental shelf. In G. Spezie and G.M.R. Manzella (Eds.), *Oceanography of the Ross Sea-Antarctica*. Heidelberg: Springer-Verlag.
- Jacobs, S.S., and C.F. Giulivi. In press-b. Interannual ocean and sea ice variability in the Ross Sea. In S. Jacobs and R. Weiss (Eds.), *Ocean, ice, and atmosphere: Interactions at the antarctic continental margin* (Antarctic Research Series, Vol. 75). Washington, D.C.: American Geophysical Union.
- Jacobs, S., H. Hellmer, and A. Jenkins. 1996. WAIS underbelly melting at Pine Island Glacier? In H. Oerter (Ed.), *Filchner-Ronne Ice Shelf Programme* (Report 10). Bremerhaven, Germany: Alfred-Wegener-Institute.
- Jacobs, S.S., A. Jenkins, and H.H. Hellmer. 1996. On the mass balance of West Antarctica's Pine Island Glacier. In S. Colbeck (Ed.), *Glaciers, ice sheets and volcanoes: A tribute to Mark F Meier* (Special Report 96-27). Hanover, New Hampshire: Cold Regions Research and Engineering Laboratory.
- Keys, H.J.R., S.S. Jacobs, and L.W. Brigham. In press. Continued northward expansion of the Ross Ice Shelf. *Annals of Glaciology*, 27.

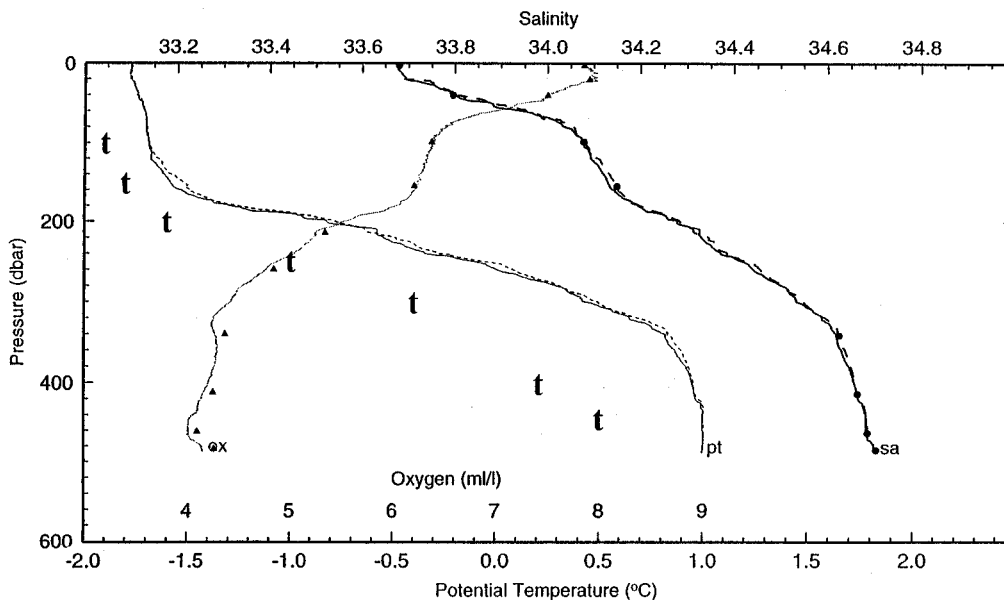


Figure 3. CTD temperature (pt), salinity (sa), and dissolved oxygen (ox) versus pressure (in decibars) from *Palmer* station 9402-119 on 21 March 1994 at 71°31'S 85°19'W. Solid symbols on the downcast oxygen profile and upcast (dashed) salinity profile indicated "bottle" values. The "t" symbols show temperatures at and below 100 meters from *Belgica* station 19 on 2 March 1898, occupied at the same location on the Bellingshausen Sea continental shelf.

Modeling tides in the Weddell and Scotia Seas

Laurie Padman, *Earth and Space Research, Seattle, Washington 98102-3620*

Robin Robertson, *College of Oceanic and Atmospheric Sciences, Oregon State University, Corvallis, Oregon 97331-5503*

We have built an eight-constituent, nonlinear, finite-difference model of barotropic tides in the Weddell and Scotia Seas and have used this model to investigate some possible effects of tides on the large-scale circulation and hydrography of the region. We summarize the model, then consider the influence of tides on the generation of mixing in the pycnocline, particularly near the shelf break and near the ice front of the Filchner–Ronne Ice Shelf (FRIS).

Model

The model is described in detail in Robertson, Padman, and Egbert (in press). In brief, the domain extends from 83°10'S to 55°00'S and from 84°00'W to 10°00'E, thus including the ocean cavities under the FRIS and other ice shelves. Over most of the domain, we obtained bathymetry from the ETOPO-5 database, which provides depths on a 1/12° global grid, but modifications to the model bathymetry were made in several regions where more recent data have become available. Bathymetry based on satellite altimetry and aircraft gravimetric surveys, as well as depth measurements from Ice Station Weddell (LaBrecque and Ghidella 1992) was used in the western Weddell Sea in the region 73°S to 65°S and 60°W to 44°W. Under the FRIS, measurements of water-column thickness were used instead of bathymetry (Vaughan et al. 1994). An Arakawa-C grid was used, with a grid spacing of 1/6° in longitude and 1/12° in latitude, resulting in a 565 × 339 array.

For this first modeling effort, we chose a two-dimensional, depth-integrated barotropic model, therefore ignoring variations of currents with depth. The model uses the mass conservation and depth-integrated shallow-water momentum equations, including the pressure and coriolis terms, astronomical forcing, bottom friction, and lateral viscosity. Eight tidal constituents were modeled, four semidiurnal and four diurnal. For land boundaries, both the no-normal flow and no-slip conditions were used. At open ocean boundaries, we used tide-height coefficients obtained from “TPXO.3,” an updated version of the global inverse tidal solution described in Egbert, Bennett, and Foreman (1994) and based on assimilation of approximately 3 years of TOPEX/Poseidon altimetry data. After model stabilization, the elevation time series were harmonically analyzed for 45 days, producing fields of the amplitude and phase for each tidal constituent. The velocity components were also harmonically analyzed for 45 days to obtain estimates of the major and minor axes, inclination, and phase for the tidal ellipses.

Principal results

Our primary interest in Weddell Sea tides is in their potential to lead to mixing of various water masses. This expectation of mixing is based on our experience with ocean

turbulence data collected in the Arctic Ocean (see Padman 1995) and the hypothesis of Foster, Foldvik, and Middleton (1987) that ocean mixing near the shelf break in the Weddell Sea might be greatly enhanced by tides. There are several dynamical mechanisms by which tides can lead to mixing, but most are too complicated to explain in useful detail in this report. Instead, we consider here only essentially qualitative estimates of the potential for mixing as a function of geographic location.

The simplest correlation we can imagine is between mixing and total tidal energy density. This latter measure can be usefully understood in terms of a spatially dependent average tidal current speed, $\langle U(x,y) \rangle$, that is calculated from time series based on all modeled tidal constituents (figure). Typical values over the deep basins are small, frequently less than 3 centimeters per second (cm s^{-1}). Over the continental shelves, $\langle U(x,y) \rangle$ normally exceeds 10 cm s^{-1} and sometimes exceeds 1 meter per second (m s^{-1}). The largest values can occur at quite strategic locations for significant mixing processes in the Weddell Sea. For example, energetic tidal currents (predominantly semidiurnal) occur at the front of the FRIS. These currents perform a dual function of not only creating mixing where Ice Shelf Water and Western Shelf Water interact but also straining the sea-ice cover and, thus, permitting a greater coupling between the ocean and atmosphere. Another region of considerable interest is around the southern shelf break, where much of the mixing of water masses that determines the ultimate temperature-salinity properties of Weddell Sea Bottom Water and Antarctic Bottom Water occurs. In particular, note the very high currents near General Belgrano Bank; currents here are primarily associated with diurnal tides.

A more complicated, but still essentially qualitative, model of mixing by tides via internal tide generation (Sjöberg and Stigebrandt 1992) has been applied by us to the Weddell Sea to map the likely mixing “hot spots.” A simple calculation in which all the generated baroclinic tidal energy is dissipated through diapycnal mixing in the pycnocline predicts a regional mean heat flux of about 20 watts per square meter (W m^{-2}) in the Weddell Sea, consistent with recent estimates of the heat loss from the Warm Deep Water (WDW) in the Weddell Gyre. As expected, mixing is concentrated near the upper slope, particularly in the southern Weddell Sea. The Sjöberg and Stigebrandt (1992) model, unfortunately, cannot deal with forced baroclinic tides south of each tidal constituent's “critical latitude,” i.e., the latitude at which the constituent's frequency equals the local coriolis frequency, nor does it allow for a flux of tidal energy into higher frequency internal waves that could then also contribute to mixing rates (Padman 1995). We are, therefore, now concentrating on running a more realistic, ver-

tically stratified numerical model forced offshore by the principal semidiurnal barotropic tide (M_2), and preliminary results suggest that mixing will be very intense near the M_2 critical latitude of $74^{\circ}29'S$, which lies near the oceanographically important southern shelf break.

Conclusions

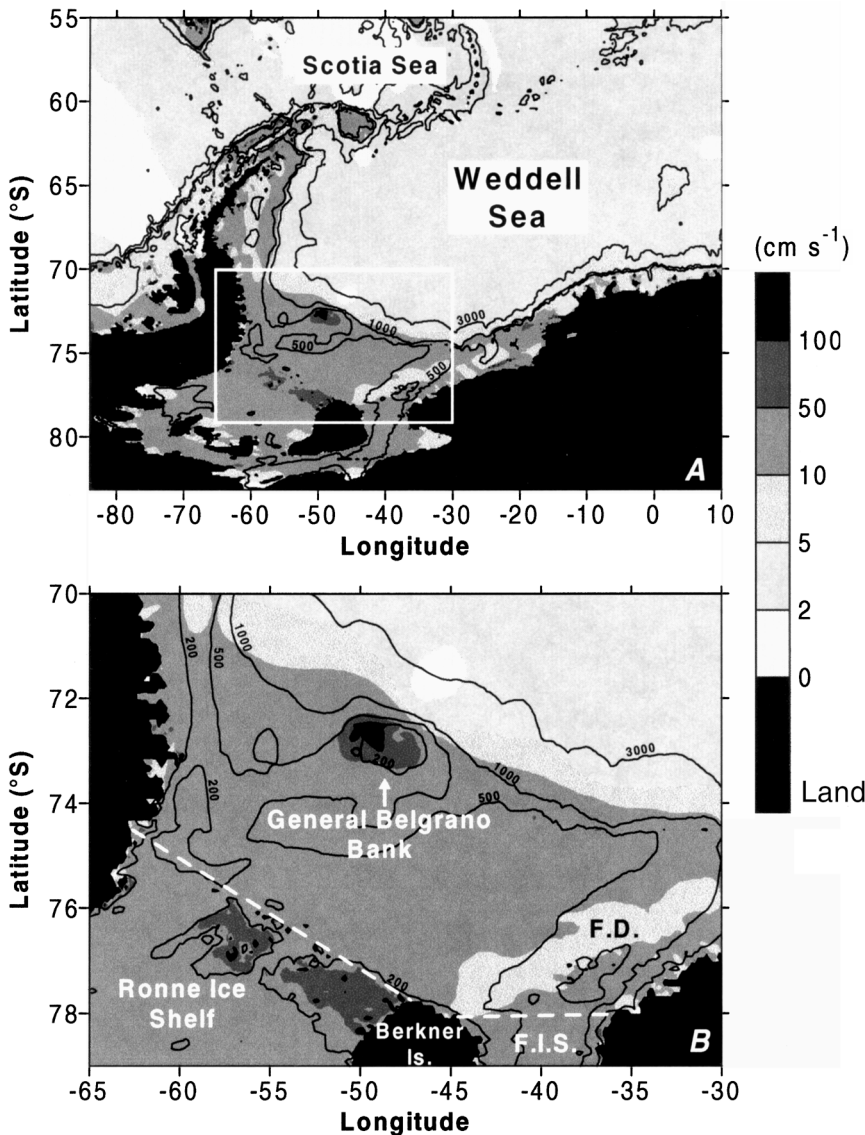
We have not yet run our tidal model coupled to a general circulation (wind- and thermohaline-forced) model or with realistic sea-ice cover. Our results to date demonstrate, however, that tides are a major component of the total oceanic kinetic energy in the Weddell Sea and may dominate as the source of turbulent kinetic energy and mixing in regions of sig-

nificant water mass formation and modification. For these reasons, plus the tides' ability to modify sea-ice characteristics such as average concentration and roughness, we conclude that tides cannot be neglected in attempts to quantify the formation rates of such globally significant water masses as Antarctic Bottom Water. Finally, we note that sensitivity studies by us indicate that the poor available bathymetric information, particularly for the southern and western shelves, is a critical limiting factor to our ability to model tides accurately. Increasing the physical sophistication of models cannot overcome the deficiencies caused by the poor bathymetry.

This research was supported by National Science Foundation grants OPP 93-17319 and OPP 96-15524.

References

- Egbert, G.D., A.F. Bennett, and M.G.G. Foreman. 1994. TOPEX/POSEIDON tides estimated using a global inverse model. *Journal of Geophysical Research*, 99(C12), 24821–24852.
- Foster, T.D., A. Foldvik, and J.H. Middleton. 1987. Mixing and bottom water formation in the shelf break region of the southern Weddell Sea. *Deep-Sea Research*, 34, 1771–1794.
- LaBrecque, J.L., and M.E. Ghidella. 1992. Estimates of bathymetry, depth to magnetic basement, and sediment thickness for the western Weddell Basin. *Antarctic Journal of the U.S.*, 27(5), 68–70.
- Padman, L. 1995. Small-scale physical processes in the Arctic Ocean. In W.O. Smith and J.M. Grebmeier (Eds.), *Arctic oceanography: Marginal ice zones and continental shelves. Coastal and estuarine studies* (Antarctic Research Series, Vol. 49). Washington, D.C.: American Geophysical Union.
- Robertson, R., L. Padman, and G.D. Egbert. In press. Tides in the Weddell Sea. In S. Jacobs and R. Weiss (Eds.), *Oceans, ice, and atmosphere: Interactions at the antarctic continental margin* (Antarctic Research Series Vol. 75). Washington, D.C.: American Geophysical Union.
- Sjöberg, B., and A. Stigebrandt. 1992. Computations of the geographical distribution of the energy flux to mixing processes via internal tides and the associated vertical circulation in the ocean. *Deep-Sea Research*, 39, 269–291.
- Vaughan, D.G., J. Sievers, C.S.M. Doake, G. Grikurov, H. Hinze, V.S. Pozdeev, H. Sandhäger, H.W. Schenke, A. Solheim, and E. Thyssen. 1994. *Map of the subglacial and seabed topography; Filchner-Ronne-Schelfeis/Weddell Sea, Antarktis, scale 1:2,000,000*. Frankfurt am Main, Germany: Institut für Angewandte Geodäsie.



Mean tidal current speed for the eight-constituent Oregon State University barotropic tidal model. (A) The full model domain is shown, and the 500-, 1,000-, and 3,000-m isobaths are indicated. (B) As in A, but for a limited region including the southern shelf and Filchner–Ronne Ice Shelf front. The Filchner Ice Shelf (F.I.S.) and Filchner Depression (F.D.) are indicated. The 200-m isobath has been added. Dashed lines indicate the approximate ice front. Note that, in our model, water depth under the ice shelves is replaced by “water column thickness.”

Global modeling of particle-reactive chemical species in the oceans: Thorium-230 advection and flux to sediment

GIDEON M. HENDERSON, *Lamont-Doherty Earth Observatory of Columbia University, Palisades, New York 10964*

CHRISTOPH HEINZE, *Max-Planck-Institut für Meteorologie, Hamburg, Germany*

ROBERT F. ANDERSON, *Lamont-Doherty Earth Observatory of Columbia University, Palisades, New York 10964*

Many chemical species exhibit particle-reactive behavior in seawater and are removed from the oceans largely by adhering to particles as they settle through the water column. In the southern oceans, these particle-reactive species are important for a number of reasons. For instance, particle-reactive pollutants such as lead and plutonium are transported from elsewhere in the oceans to this relatively pristine environment and removed there by high particle fluxes. The biolimiting nutrient iron also exhibits particle-reactive behavior that controls its rate of advection into the iron-poor southern oceans, and several particle-reactive radioactive nuclides are proving useful in this important region as proxies for past global change. Examples of the latter include the use of thorium-230 (^{230}Th) as a constant flux indicator to assess accumulation rates of southern-ocean sediment constituents, and the use of protactinium-231/thorium-230 ($^{231}\text{Pa}/^{230}\text{Th}$) ratios to indicate past productivity (Kumar et al. 1995) or ocean-circulation (Yu, Francois, and Bacon 1996).

Several attempts have been made to model particle-reactive species for single ocean profiles, but global models of the advection and removal of these species have not been constructed. Such models, however, could offer key constraints on the rate of advection of particle-reactive species, their flux to ocean sediments, and their use as proxies of global change. As a first step toward incorporating particle-reactive species into global ocean models, we have focused on ^{230}Th , which has several advantages for this purpose.

- It is produced uniformly throughout the oceans by the decay of well-mixed uranium.
- It is one of the most highly particle-reactive elements so that its oceanic behavior is completely dominated by particle reactivity.
- It has been widely studied; over 800 existing measurements of oceanic ^{230}Th concentrations have been made, and its chemical behavior in seawater is well understood.

We have used two previously described global ocean models. The Large-Scale Geostrophic Ocean General Circulation Model (Maier-Reimer, Mikolajewicz, and Hasselmann 1993) derives ocean circulation, and the Hamburg Oceanic Carbon Cycle Model (Maier-Reimer 1993) produces surface-ocean productivity. To these models, we have added subroutines that accurately parametrize the settling of surface-derived particles through the water column and the removal of particle-reactive species onto these particles as they settle. A manuscript describing this work is in preparation and further details are available at <http://www.ldeo.columbia.edu/~gideon/>,

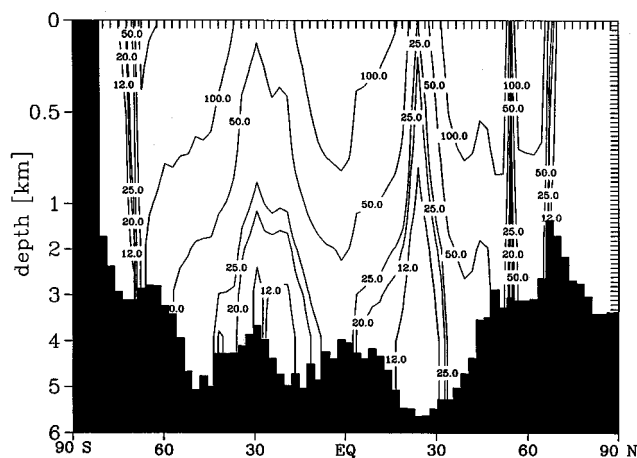


Figure 1. Model-derived particle concentrations in micrograms per liter for the western Atlantic Geochemical Ocean Sections Study (GEOSECS) section. Absolute values and the distribution of concentrations agree well with observed values.

together with a collation of all existing water-column ^{230}Th measurements.

The accuracy of the particle field produced by the model is illustrated in figure 1 by a meridional section of the western Atlantic. Absolute values produced by the model agree well with those of Brewer et al. (1976), and the pattern of particle concentration here, and elsewhere in the Atlantic, agrees well with that measured by nephelometry (Biscaye and Eitrem 1977). The accuracy of the ^{230}Th handling is assessed by comparison with existing water-column measurements. Average depth profiles of model ^{230}Th concentration, both in the dissolved and particle phases, agree well with the average of observed values, increasing from close to 0 at the surface to values of approximately 1 decay per minute per 1,000 liters dissolved ^{230}Th at 5 kilometers (km). Comparison of model results with individual observed profiles demonstrates that the model is generally advecting and removing ^{230}Th realistically. A particular success is the replication of low ^{230}Th concentrations in the Labrador Sea; these low concentrations result from the advection to depth of low ^{230}Th surface waters (Moran et al. 1997). The model-to-observation fit is less good, however, in the far southern oceans. Here, observed ^{230}Th values are high, probably due to advection of water from the Weddell Sea where particle fluxes are very low and ^{230}Th concentrations correspondingly high (Rutgers van der Loeff and

Berger 1993). Model values in the far southern oceans are not, however, significantly higher than elsewhere, probably reflecting insufficient resolution in the present model to replicate accurately the complex circulation and sea-ice dynamics of the southern oceans.

Despite its failings in the far southern oceans, the model's accurate duplication of water-column ^{230}Th values elsewhere suggests that it is advecting and removing ^{230}Th realistically over most of the globe. This accuracy allows us to construct a global map of the removal of ^{230}Th to ocean sediment relative

to ^{230}Th production in the overlying water column (figure 2). This map shows that, in regions where productivity is low, less ^{230}Th is removed to the sediment than is produced there. The extra ^{230}Th is advected from these areas to be removed in areas of high productivity. The magnitude of this effect is such that up to half of the ^{230}Th produced is advected in the most extreme cases.

Another run of the model was performed using Last Glacial Maximum boundary conditions (Winguth et al. 1996). Major features of the Glacial ^{230}Th flux map (figure 3) are similar to those of the Holocene

with the notable exception that additional ice cover during the Last Glacial Maximum reduces removal of ^{230}Th in the Arctic and, therefore, increases its removal in the North Atlantic and North Pacific. The Holocene and Last Glacial Maximum models demonstrate that the use of ^{230}Th as a constant flux indicator in ocean sediments must be treated with some care to be interpreted at high precision.

Further work will refine the model in the southern oceans. Ongoing Joint Global Ocean Flux Studies (JGOFS) will help in this regard by improving understanding of the particle fluxes in the seasonal ice zone. The model will also be used to investigate other particle-reactive species. In particular, ^{231}Pa has been introduced to the model to test the interpretation of $^{231}\text{Pa}/^{230}\text{Th}$ results from southern ocean sediments as proxies for past productivity (Kumar et al. 1995) and/or ocean circulation (Yu et al. 1996). Further work will also introduce beryllium-10 (^{10}Be) and possibly particle-reactive pollutants to investigate their advection into, and removal from, the southern oceans.

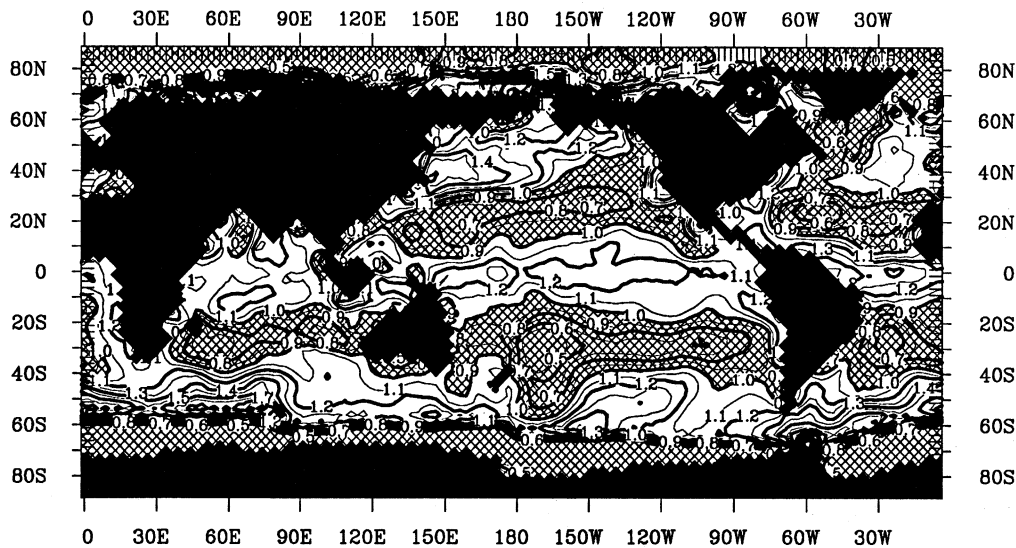


Figure 2. Model-derived Holocene ^{230}Th flux-to-sediment relative to production in the overlying water column. Cross-hatched regions are those in which less ^{230}Th is removed from the water column than is produced there and are situated in regions of low productivity.

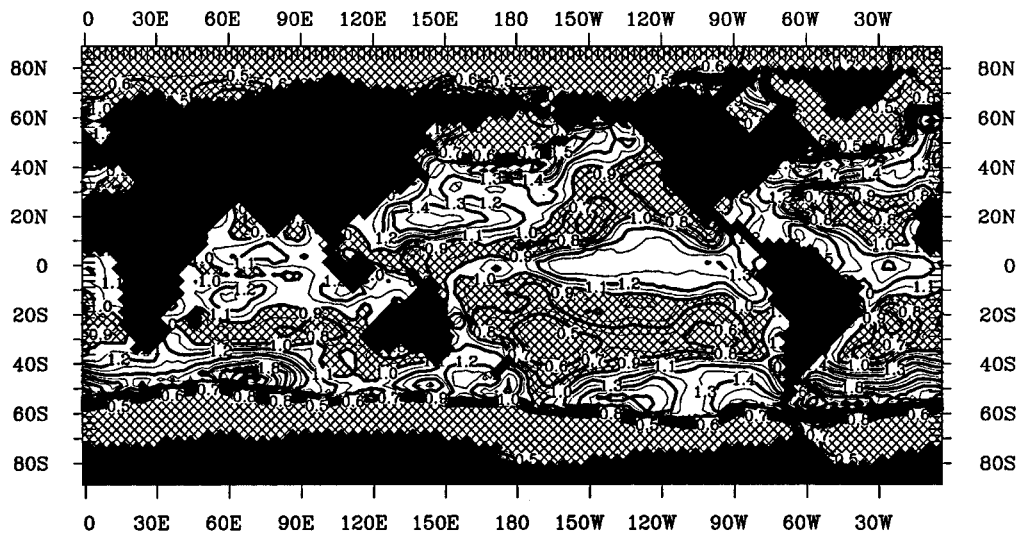


Figure 3. Model-derived Last Glacial Maximum ^{230}Th flux-to-sediment relative to production in the overlying water column. Details as figure 2 but note the reduced removal in the Arctic and correspondingly higher removal in the North Atlantic and Pacific.

References

- Biscaye, P.E., and S.L. Eittrheim. 1977. Suspended particulate loads and transports in the nepheloid layer of the abyssal Atlantic Ocean. *Marine Geology*, 23, 155–172.
- Brewer, P.G., D.W. Spencer, P.E. Biscaye, A. Hanley, P.L. Sachs, C.L. Smith, S. Kadar, and J. Fredericks. 1976. The distribution of particulate matter in the Atlantic Ocean. *Earth and Planetary Science Letters*, 32, 393–402.
- Kumar, N., R.F. Anderson, R.A. Mortlock, P.N. Froelich, P. Kubik, B. Dittrich-Hannen, and M. Suter. 1995. Increased biological productivity and export production in the glacial southern ocean. *Nature*, 378, 675–680.
- Maier-Reimer, E. 1993. Geochemical cycles in an ocean general circulation model: Preindustrial tracer distributions. *Global Biogeochemical Cycles*, 7(3), 645–677.
- Maier-Reimer, E., U. Mikolajewicz, and K. Hasselmann. 1993. Mean circulation of the Hamburg LSG OGCM and its sensitivity to the thermohaline surface forcing. *Journal of Physical Oceanography*, 23, 731–757.
- Moran, S.B., M.A. Charette, J.A. Hoff, R.L. Edwards, and W.M. Landing. 1997. Distribution of ^{230}Th in the Labrador Sea and its relation to ventilation. *Earth and Planetary Science Letters*, 150, 151–160.
- Rutgers van der Loeff, M.M., and G.W. Berger. 1993. Scavenging of ^{230}Th and ^{231}Pa near the Antarctic Polar Front in the South Atlantic. *Deep-Sea Research*, 40(2), 339–357.
- Winguth, A.M.E., E. Maier-Reimer, U. Mikolajewicz, and J.-C. Duplessy. 1996. On the sensitivity of an ocean general circulation model to glacial boundary conditions. *Max-Planck-Institut für Meteorologie Internal Report*. Hamburg, Germany: Max-Planck-Institut.
- Yu, E.F., R. Francois, and M. Bacon. 1996. Similar rates of modern and last-glacial ocean thermohaline circulation inferred from radiochemical data. *Nature*, 379, 689–694.